SIMULATION OF A HEAVY WINTERTIME PRECIPITATION EVENT IN CALIFORNIA

SU-TZAI SOONG
Dept. of Land Air and Water Resources, Univ. California, Davis, CA 95616, U.S.A.

and

JINWON KIM
Lawrence Livermore National Laboratory, L-262, Univ. California, P.O. Box 808, Livermore, CA 94551, U.S.A.

Abstract. A coupled mesoscale atmospheric-land surface model is used to simulate a twelve-day heavy precipitation event in California. In addition to the temporal variation of the large-scale flow, local topography played a crucial role in the simulated precipitation and land-surface snow budget through orographically-generated vertical motion and a decrease of atmospheric temperature with increasing altitude. The observed and simulated heavy precipitation occurred at locations where orographic lifting is strong: western slopes of the Sierra Nevada Mountains and the Coastal Range. Due to rainshadow effects, the Central Valley area, which is located at the lee side of the Coastal Range, received only a small amount of precipitation. The snowline appeared at altitudes as low as 750 m above sea level, and most of the precipitation above the 1.8 km level was snow. Maximum rainfall was located near the 1 km elevation along the western slope of the Sierra-Nevada while snowfall maxima appeared along the ridge of the Sierra Nevada Mountains. Snow accumulation was also strongly dependent upon surface elevations. The simulation suggested that over 75% of the fresh snowfall during the study period was added to the existing snow cover at elevations above 1.5 km while much of the snowfall over lower elevations melted.

1. Introduction

Accurate diagnosis and prediction of precipitation are important tasks for improvements in water resources management and surface hydrology forecasts over various time scales. Accurate estimations of snowfall and snow accumulation during winter months are especially important in California since the snowpack at high elevations is the major source of water supply during dry summer months (Chen *et al.*, 1994). Precipitation over the western United States has been an important subject of many numerical studies in recent years (Giorgi and Bates, 1989; Dickinson *et al.*, 1989; Giorgi, 1990; Giorgi *et al.*, 1993a). For accurate simulations of air flows and precipitation over steep and complex terrain such as the western United States, a model must include an accurate advection scheme and physically-based parameterizations of precipitation processes. In California, the topography exerts important controls on the amount, spatial distribution, and the occurrence of rainfall and snowfall. These characteristics of precipitation in the western United States require a model capable of handling steep orography and correctly accounting for the total precipitation and its partitioning into rainfall and snowfall. Rapidly changing synoptic

Climatic Change **32:** 55–77, 1996.

flows during the periods of intense storm also require a model to accurately handle time-dependent large-scale flows, especially for long term simulations (Errico and Baumhefner, 1987; Giorgi and Bates, 1989; Giorgi *et al.*, 1993b).

A well-designed advection scheme which minimizes numerical dispersion is highly desirable for simulating airflows and precipitation over complex terrains. Steep and complex terrain and local condensation introduce strong spatial gradients in the atmospheric flow fields, and strong spatial gradients are major causes of spurious numerical dispersion and noise in the simulated flow fields. This noise can lead to fictitious condensation, inaccurate water budget estimates, and, often, numerical instability. Numerical dispersion is usually controlled by numerical diffusion. However, excessive numerical diffusion may smooth out important local features associated with complex terrain and condensational heating.

Physically-based parameterizations of the grid-scale condensation and precipitation are important for accurately simulating precipitation and surface hydrology in California. Major portion of winter precipitation in California is from stratiform clouds associated with storms originating in the eastern Pacific. Even though imbedded convective precipitation is important for causing localized heavy precipitation and flash flood, most of the wintertime precipitation in California is associated with relatively shallow stratocumulus clouds. Accurate estimates of rainfall and snowfall, which are important for short- and long-term surface hydrology, also require correct treatments of cloud microphysical processes.

Until recently, grid-scale precipitation has been computed by employing a variety of isobaric condensation schemes (Haltiner and Williams, 1980; Giorgi, 1990) which are simple to formulate and inexpensive to run. However, they treat important precipitation processes, such as the fallout and re-evaporation of precipitating particles, in somewhat arbitrary ways. These uncertainties can cause significant amounts of error in the simulated precipitation. For example, a large portion of wintertime precipitation in California is snow. Large differences between the fall speeds of rain and snow particles can significantly contribute to the spatial distribution of precipitation through downstream transport of snow particles. Partitioning the total precipitation into rain and snow by considering the ambient temperature (e.g., Giorgi and Bates, 1989) can not account for differences between the fall speeds of raindrops and snow particles. In addition, ice phase processes have strong effects on the formation of precipitation and vertical distributions of the heating and cooling due to condensation, freezing, and melting (Choularton and Perry, 1986; Dudhia, 1989). Neglecting these effects can cause significant errors in the simulated thermal forcing due to condensation and re-evaporation.

Recently, bulk parameterization of cloud microphysics, that has been an essential component of cloud modeling, have become to be widely used for computing the grid-scale condensation in primitive equation mesoscale models (Zhang *et al.*, 1988, 1989; Zhang and Fritsch, 1988; Zhang and Gao, 1989; Giorgi, 1991; Giorgi *et al.*, 1993b). By employing a parameterized microphysics, many details of microphysical processes can be accounted for in computing the grid-scale precipitation.

Previous numerical studies showed that including a parameterized microphysics significantly improved the simulations of storm-related mesoscale features such as the evolution of a mesovortex and squall lines.

The amount of snowpack varies due to the difference between the fresh snowfall and snowmelt during a given period. Since snowmelt is one of the major components of the surface energy and hydrology budget over snow-covered surfaces, an estimation of the amount of water stored in snowpack needs accurate computations of the energy and hydrological balances at land surfaces. Even though bucket-type models have been widely used in many regional and global studies, they lack important physical processes associated with soil hydrology and evapotranspiration. Thus, in addition to physically-based precipitation parameterizations, a land-surface model which includes detailed physical processes for evapotranspiration and soil hydrology, is required for correctly estimating the variation of snowpack during the course of winter seasons.

In Section 2, we present descriptions of the coupled atmospheric-land surface simulation model employed in this study. Section 3 describes the outline of this numerical experiment. In Sections 4 and 5, we present the simulated precipitation and variations of snowpack during the simulation period.

2. Model Description

The Mesoscale Atmospheric Simulation (MAS) model we have used in this study is a primitive-equation, limited-area model intended primarily to simulate regional atmospheric and land-surface processes. The governing equations are the flux-form of the primitive equation written on σ-coordinates (e.g., Anthes and Warner, 1978):

$$\frac{\partial(\pi u)}{\partial t} = -m^2\left[\frac{\partial}{\partial x}\left(\frac{\pi uu}{m}\right)+\frac{\partial}{\partial y}\left(\frac{\pi vu}{m}\right)\right]+\pi(f+\gamma)v - \frac{\partial(\pi\dot{\sigma}u)}{\partial\sigma} - m\left(\frac{\partial\phi}{\partial x}-\sigma\frac{\partial\phi}{\partial\sigma}\frac{\partial\pi}{\partial x}\right)+\pi F_x \tag{1}$$

$$\frac{\partial(\pi v)}{\partial t} = -m^2\left[\frac{\partial}{\partial x}\left(\frac{\pi uv}{m}\right)+\frac{\partial}{\partial y}\left(\frac{\pi vv}{m}\right)\right]+\pi(f+\gamma)u - \frac{\partial(\pi\dot{\sigma}v)}{\partial\sigma} - m\left(\frac{\partial\phi}{\partial y}-\sigma\frac{\partial\phi}{\partial\sigma}\frac{\partial\pi}{\partial y}\right)+\pi F_y \tag{2}$$

$$\mathrm{d}\phi = -C_\mathrm{p}\theta\mathrm{d}P \tag{3}$$

$$\frac{\partial(\pi\theta)}{\partial t} = -m^2\left[\frac{\partial}{\partial x}\left(\frac{\pi u\theta}{m}\right)+\frac{\partial}{\partial y}\left(\frac{\pi vy}{m}\right)\right]-\frac{\partial(\pi\dot{\sigma}\theta)}{\partial\sigma}+\pi Q \tag{4}$$

$$\frac{\partial(\pi q)}{\partial t} = -m^2\left[\frac{\partial}{\partial x}\left(\frac{\pi uq}{m}\right)+\frac{\partial}{\partial y}\left(\frac{\pi vq}{m}\right)\right]-\frac{\partial(\pi\dot{\sigma}q)}{\partial\sigma}+\pi S \tag{5}$$

$$\frac{\partial \pi}{\partial t} = -m^2 \left[\frac{\partial}{\partial x} \left(\frac{\pi u}{m} \right) + \frac{\partial}{\partial y} \left(\frac{\pi v}{m} \right) \right] - \frac{\partial (\pi \dot{\sigma})}{\partial \sigma} \tag{6}$$

$$\gamma = -v \frac{\partial m}{\partial x} + u \frac{\partial m}{\partial y}$$

where m is the map factor, $\pi = p_{\text{sfc}} - p_{\text{top}}$, $P = (p/p_0)^{R_d/C_p}$, Q the diabatic heating rate, and S is the net source/sink of a tracer variable q such as water vapor, condensed water, and other pollutants, and F_x and F_y are non-conservative forcing on the x- and y-component of momentum, respectively. The curvature term γ in Equations (1)–(2), is much smaller than the Coriolis parameter in middle latitudes and may be neglected (Anthes and Warner, 1978). Other symbols in Equations (1)–(6) have conventional meanings (e.g., Arakawa and Suarez, 1983). The continuity equation (6) is integrated vertically to yield the surface pressure tendency equation (Arakawa and Suarez, 1983):

$$\frac{\partial \pi}{\partial t} = -m^2 \int_{\sigma=1}^{\sigma=0} [\partial(\pi u/m)/\partial x + \partial(\pi v/m)/\partial y] \mathrm{d}\sigma \tag{7}$$

The governing equations (1)–(7) are discretized on the Arakawa c-grid. To solve the flux form of the advection equation, we employ the third-order accurate, finite-difference scheme which was initially developed by Takacs (1985) and later modified by Hsu and Arakawa (1990). This advection scheme is nearly positive-definite and causes minimal amounts of phase error and numerical dispersion. These numerical characteristics are important advantages for simulating atmospheric flows over complex terrains. Except for the advection part of the governing equations, we employ forth-order accurate, centered finite difference schemes to compute horizontal differentiations (e.g., computing pressure gradient force) at the interior of the model domain. Dependent variables are staggered in the vertical using the Lorenz grid (Arakawa, 1986) with the vertical differencing scheme introduced by Arakawa and Suarez (1983).

To represent temporal variations of large-scale flow, we imposed time-dependent lateral boundary conditions obtained from large-scale data using a Davies-type relaxation scheme (Davies, 1976). Giorgi *et al.* (1993b) provided detailed description of an application of this scheme to a mesoscale climate model.

Precipitation processes are computed separately for the convective precipitation and the grid-scale precipitation. To compute the grid-scale precipitation, we employed a bulk cloud microphysics parameterization by Cho *et al.* (1989). This scheme accounts for interactions between water vapor and five classes of hydrometeors that include cloud water, cloud ice, rain, snow, and graupel. It neglects hail or large graupel particles which may be important for simulating deep convective system (Lin *et al.*, 1983) but are not important for shallow clouds. Details of this microphysics formulation were presented by Cho and Iribarne (1987) and Cho *et al.* (1989) and will not be discussed here. We employ a Kuo-type cumulus parameterization (Kuo, 1965; Krishnamurti *et al.*, 1980) to compute the precipitation

and thermal forcing due to convective clouds. To conserve total moisture and heat exchange due to phase change of water substances, the cloud microphysics and cumulus parameterizations are applied in such a way that the model atmosphere is first adjusted by applying cumulus parameterization and the adjusted temperature and moisture fields are used to compute microphysical processes. Reversing the order of application did not cause noticeable differences. Even though embedded convection is important for locally concentrated heavy precipitation, our tests showed that the simulated precipitation in this case study was mainly produced by the microphysics scheme. Further investigation of the sensitivity of the simulated precipitation on various cumulus convection schemes is being performed.

Solar and terrestrial radiative transfer are computed using multi-layer schemes by Davis (1982) and Harshvardhan and Corsetti (1984), respectively, after they are modified to include the effects of clouds. The solar radiative transfer model is a broad-band scheme that divides the frequency range of the solar spectrum into seven bands. It employs the Delta-Eddington (two-stream) approximation for large (small) optical thickness. More details of this solar radiation model are presented by Lacis and Hansen (1974), Davis (1982), and Harshvardhan *et al.* (1987). The terrestrial radiative transfer model computes bulk emissivity of a model layer in the presence of water vapor, ozone, and carbon dioxide in the clear sky. Details of this scheme can be found in Harshvardhan and Corsetti (1984) and Harshvardhan *et al.* (1987). Effects of clouds on the solar and terrestrial radiative transfer are computed by considering water and ice particles separately using the formulations by Stephens (1978) and Starr and Cox (1985), respectively. Amounts of cloud particles within a model layer are directly computed by the cloud microphysics formulation employed in the MAS model. This is another advantage of including an explicit cloud microphysics formation in the MAS model. We do not consider partial cloudiness in computing radiative transfer, hence an entire grid box is filled with clouds whenever condensed water is present in that grid.

Vertical turbulent transfer of momentum, heat, and tracers at the surface are computed by the bulk aerodynamic transfer scheme (Deardorff, 1978). The surface fluxes of momentum, with a no-slip lower boundary condition, and a scalar variable ϕ are computed as

$$(\overline{u'w'})_s = -C_D|\vec{V}_0|u_0 \tag{8a}$$

$$(\overline{v'w'})_s = -C_D|\vec{V}_0|v_0 \tag{8b}$$

$$(\overline{\phi'w'})_s = -C_H|\vec{V}_0|(\phi_0 - \phi_s) \tag{8c}$$

where C_H and C_D are the surface drag coefficients for heat and momentum, respectively. The subscripts s and 0 denote the values at the surface and at the reference atmospheric level, respectively. The surface drag coefficients for other scalar variables such as water vapor are assumed to be the same as that for heat. We also assume that the surface layer extends over the entire lowest model layer to avoid

extrapolating atmospheric variables to obtain the near-surface wind and other variables. Vertical turbulent transfer outside the surface layer is computed using a K-theory as

$$(\overline{\phi' w'})(z) = -\frac{\partial}{\partial z}\left[K_{\mathrm{m,h}}\frac{\partial \phi}{\partial z}\right] \tag{9}$$

where ϕ is any dependent variable and K_{m} and K_{h} are eddy diffusivities for momentum and heat, respectively. Same as for the surface drag coefficients, the eddy diffusivity for scalar variables is assumed the same as that for heat. The surface drag coefficients and eddy diffusivities are computed using the formula of Louis *et al.* (1981) which includes the effects of the atmospheric stratification and shear. The asymptotic mixing length*, necessary to close the formulation, is assumed to be 15 m following Kim and Mahrt (1992).

Temperature and mixing ratio at land surfaces, which are necessary for computing sensible and latent heat fluxes at land surfaces, are obtained by solving the surface energy balance equation. For computing the surface energy balance, we include the effects of soil water content, soil heat flux, vegetation, and snow cover by employing the Coupled Atmosphere Plant Snow (CAPS) model developed at Oregon State University (Mahrt and Pan, 1984; Ek and Mahrt, 1991; Kim *et al.*, 1994). The CAPS model predicts the soil temperature, soil water content, equivalent snow depth, and canopy water content. The CAPS model computes the total evapotranspiration from a combined soil-canopy surface by considering fractions of land-surface area covered with vegetation and bare soil. However, partial snow cover is not considered. Whenever non-zero snow cover is present within a grid, the entire area of that grid is assumed to be covered with snow. In addition to the surface temperature and mixing ratio, the CAPS model also computes runoff and accumulated snow cover.

3. Experimental Design

The case we selected for this study is marked by twelve days of heavy precipitation over the northern and central California during February 1986. This heavy precipitation caused a flood in the Sacramento Valley area. We have carried out a simulation for a twelve-day period of 00UTC 11–00UTC 23, February, 1986.

Figure 1 illustrates the vertical structure of the coupled model. The MAS model was configured with 14 irregularly-spaced atmospheric layers between the surface and the top of the computational domain. We placed the top of the computational domain at the 50-mb level to avoid extrapolating variables in the upper part of the

* This parameter represents the mixing length at neutral stratification. This value may vary depending on the horizontal resolution of individual models. A value of a few hundred meters has been typical for applications in GCMs. For mesoscale models, where the resolution is of a few tens of kilometers, the value suggested by Kim and Mahrt (1992) may be suitable.

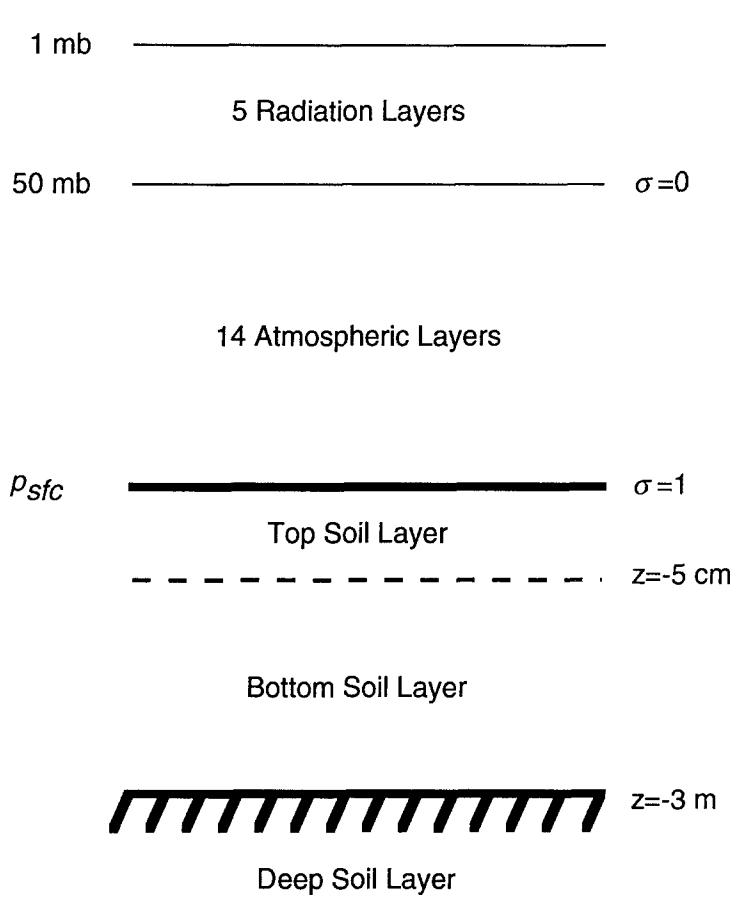

Fig. 1. The vertical structure of the coupled MAS-CAPS model employed in this study.

model domain. We added five layers between the 50-mb and 1-mb levels to compute downwelling solar and terrestrial radiation at the top of the computational domain. The CAPS model was configured with two soil layers where the top and bottom soil layers are located at 5 cm and 1 m below the ground surface, respectively. The depth of the hydrologically and thermally active soil layer was assigned to be 3 m. We assumed that vegetation uniformly covers 80% of land surfaces throughout the model domain. This value of the fractional coverage of vegetation is arbitrary and needs to be refined for long term simulations.**

The computational domain (Figure 2) covers an area of 1140 km × 1260 km in the horizontal that includes California, Nevada, and southern Oregon. This computational domain is covered with a uniform-resolution 20 km × 20 km grid mesh in the horizontal. At this horizontal resolution, major features of local orography, the Coastal Range, the Central Valley, and the Sierra Nevada Mountains, are well

** Wet soil, cold surface temperature, and low insolation made the overall evaporation during this study period less dependent on the surface vegetation.

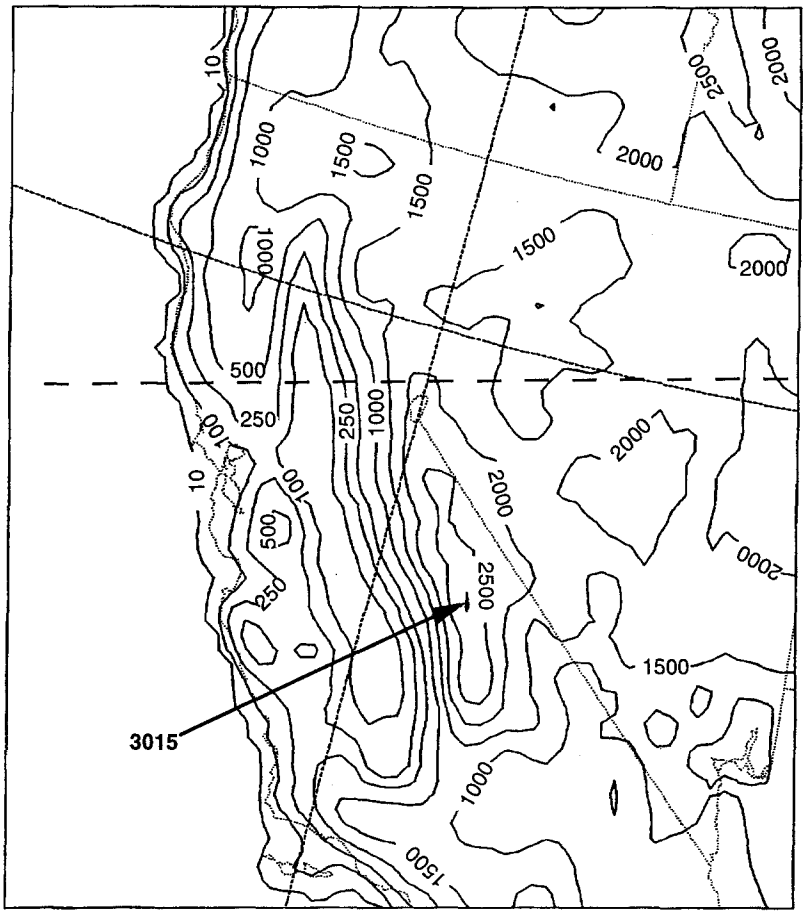

Fig. 2. Model terrain at 20 km × 20 km horizontal resolution. The dashed line indicates the location of the cross-section presented in Figure 7.

represented. However, this resolution was not fine enough to capture the narrow and steep coastal topography of California. Proper representation of the coastal topography of California may require horizontal resolutions of a few kilometers, or a special scheme, such as the envelope orography in global models (Wallace *et al.*, 1983), to define model terrain.

The initial and time-dependent lateral boundary conditions for this simulation were obtained from the twice-daily National Meteorological Center (NMC) global analysis. To represent this coarse resolution analysis data in fine-resolution mesoscale model grids, we first horizontally interpolated the 2.5° × 2.5° resolution pressure-level NMC analysis data onto 20 km × 20 km resolution MAS model grids using a Cressman objective analysis scheme (Cressman, 1959). This horizontally interpolated pressure-level data of 20 km × 20 km resolution was then vertically interpolated onto the σ-levels of the MAS model. Time-dependent lateral boundary

conditions were computed by linearly interpolating the NMC analysis data in time at every twelve-hour intervals. We used the climatological subtropical wintertime profiles of the temperature and the mixing ratios of the water vapor and ozone (Ellingson *et al.*, 1991) to compute the incident short- and longwave radiation at the top of the computational domain (50 mb) since the NMC analysis does not provide atmospheric information above the 50 mb level. The ozone mixing ratio within the computational domain (below 50 mb level) was also prescribed as a function of the height from the same data.

The CAPS model requires the soil texture and initial values of the soil temperature and soil water content. The soil texture at individual model grid points was obtained from $1° \times 1°$ resolution data by Zobler (1986) by assuming that the soil texture within a model grid is the same as that of the nearest data points. The initial value of the soil water content was obtained by linearly interpolating $1° \times 1°$ resolution climatological soil moisture data by Zobler (1986). This climatological soil moisture data is intended for bucket-type models. In order to convert it into the volumetric soil water content needed by the CAPS model, we divided the depth of water at each bucket by the saturated value (150 mm). This yields the portion of total hydrological column of soil filled with water, which is the definition of the soil water content. Since the soil temperature field was not available, we simply assumed that the soil temperature is initially the same as the air temperature near the ground surface which is obtained by vertically extrapolating the lowest-layer initial temperature using the temperature lapse rate of the U.S. standard atmosphere (6.5 K/km). The initial values of the soil temperature and soil water content thus obtained do not represent the actual state of land surfaces at the beginning of the simulation. However, uncertainties in the initial soil variables did not affect the simulated precipitation in this study since the simulated precipitation is mainly determined by the large scale water vapor flux and local topography. Wet soil, heavy precipitation, and thick cloud cover during the study period also weakened the effects of surface fluxes on the simulated precipitation and low level flows.

4. Observed Precipitation

We briefly discuss the observed spatial distribution of precipitation, daily precipitation, and relationship between the local precipitation and large-scale water vapor budget in California during the study period. Features of the observed precipitation discussed in this section are used to evaluate the simulated precipitation in the following section. Analyses of the observed twelve-day total precipitation was obtained from a report by Department of Water Resources of California (1988) as well as from the raingauge data obtained at 165 raingauge stations within California.

The observed precipitation during the twelve-day period clearly shows the effects of local orography and the large-scale water vapor flux convergence on

the spatial distribution and the total amounts of precipitation in the area. Spatial distribution of the total precipitation, which combines rainfall and snowfall, integrated over the twelve-day period (Figure 3) indicates that major mountain ranges within California caused a strong west-east gradients in the precipitation across the region. The heaviest precipitation occurred over the western slopes and ridge lines of the Sierra Nevada Mountains and the Coastal Range due to strong orographic lifting of the low-level inflow from the Pacific Ocean. Due to rainshadow effects, precipitation decreased rapidly at the lee sides of the Coastal Range and the Sierra Nevada, i.e., the Central Valley and eastern Nevada, respectively. Isolated precipitation maxima along the coast of California indicate the importance of narrow but steep coastal geometry in developing locally concentrated precipitation events.

The temporal variation of the observed precipitation in California was closely correlated with the temporal variation of the large scale water vapor budget across the model domain. The observed daily precipitation, averaged over 165 raingauges in California, varied closely with the large scale water vapor flux convergence over the model domain calculated from the NMC analysis (Figure 4). This result is consistent with the observational study of Roads *et al.* (1994) who found that atmospheric water vapor flux convergence is an important contributor to local precipitation along the U.S. west coast, especially during winter seasons. This close correlation between the local precipitation and the large scale water vapor flux convergence also implies that the NMC analysis characterizes the large-scale moisture budget over the area well during the study period.

5. Simulated Precipitation

To evaluate the simulated precipitation, we mainly compare grid-point values against rain gauge data within the grid point. A grid-point value, however, is not directly comparable to a rain gauge data since the area represented by a grid point and a rain gauge are different by many orders of magnitude. To compare the grid-point values with rain gauge values, we constructed both the area-mean and time-mean values of the observed and simulated precipitation. Roads *et al.* (1991) and Giorgi *et al.* (1993a) employed a similar approach for comparing rain gauge data and grid point data.

Figure 4 also illustrates the temporal variation of the simulated precipitation averaged over 161 model grid points which contain at least one rain gauge. Close correlations among the temporal variations of the large-scale water vapor budget and simulated and observed precipitation suggests that the Davies-type lateral boundary scheme handled well the time-dependent large-scale flows. Uncertainties in comparing the observed and simulated daily precipitation arise due to different times of accumulation between the station and the model. A day in the simulation was defined from 00UTC (4 pm PST) of a day to 00UTC of the next day. Accumulation times vary from station to station and are different from this mod-

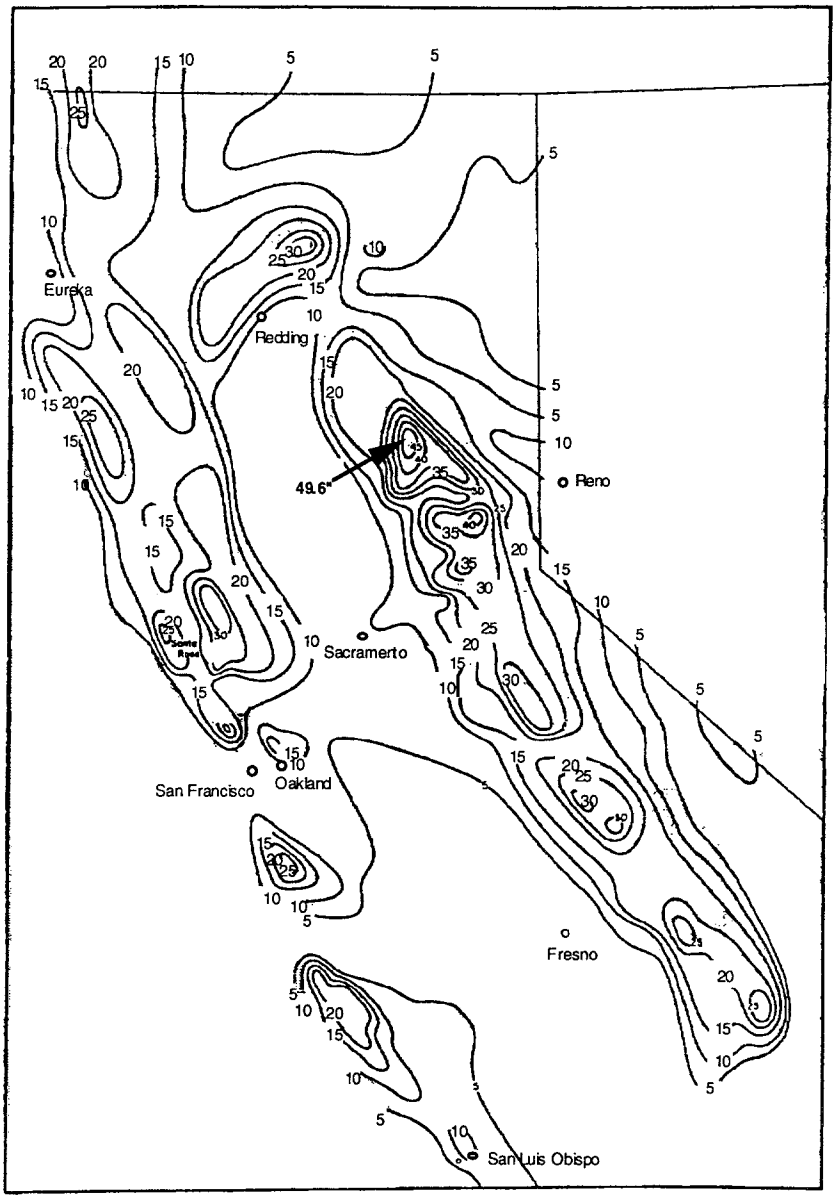

Fig. 3. An analysis of the observed 12-day total precipitation in California for 11–22, February 1986 (California Dept. of Water Resources).

el accumulation time. This can introduce significant amounts of uncertainties in comparing daily precipitation, especially when heavy precipitation is concentrated over a period of a few hours. For example, the MAS model predicted heavy precipitation during the period of 00UTC–12UTC, 18 February (4 pm 17–4 am PST 18 February). Most of this twelve-hour period belongs to the evening of 17

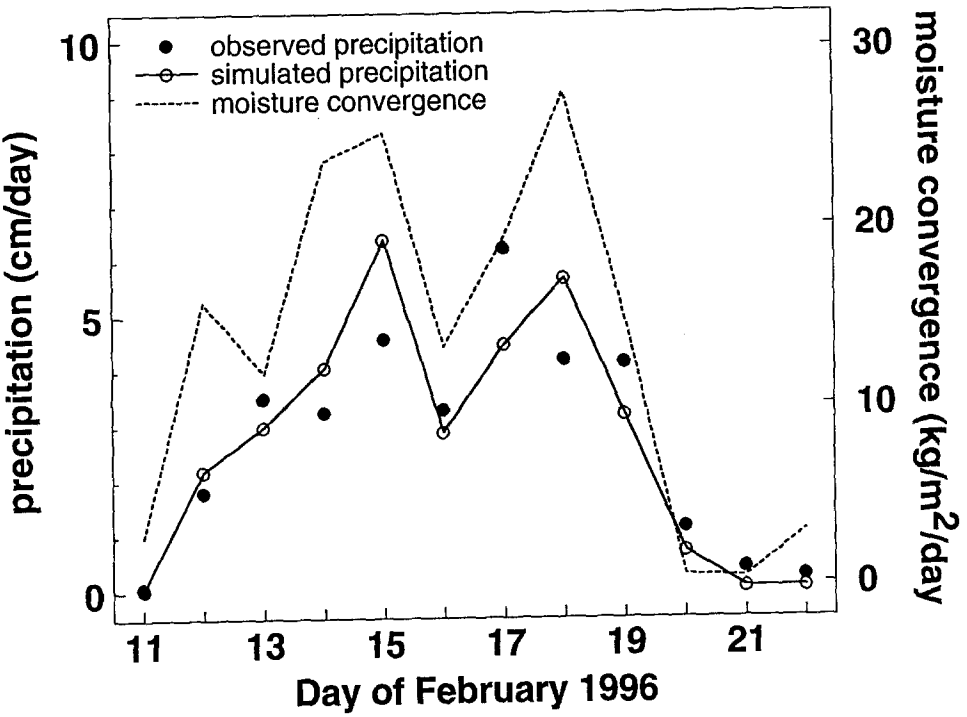

Fig. 4. Daily-mean precipitation observed at 165 raingauges in California (solid circles), simulated at 161 grid points containing rain gauges (solid line with open circles), and the large scale water vapor flux convergence across the model domain computed from the twice-daily NMC global analysis (dashed line).

February in local time, but, when daily precipitation was computed, precipitation during this period was added to 18 February. Therefore, a large portion of the simulated daily precipitation on 18 February actually occurred on 17 February. The daily precipitation on 14 and 15 February was affected similarly since heavy precipitation occurred during the period of 00UTC-12UTC, 15 February.

The spatial distribution of the simulated 12-day total precipitation (Figure 5) closely agrees with observations analyzed by California Dept. of Water Resources (Figure 3). The simulated precipitation is concentrated along the western slopes and ridge lines of the Sierra Nevada and Coastal Range with small amounts of precipitation in the Central Valley and east of the Sierra Nevada. Locations and magnitudes of the observed precipitation maxima over the Sierra Nevada and the Coastal Range are well reproduced in the simulation. The simulated 12-day total precipitation shows maximum value of 45.2 inches at the western slope of northern Sierra Nevada while the observations indicated the maximum twelve-day total precipitation of 49.6 inches near the same location.

Figure 6 compares the observed 12-day total raingauge precipitation over California with the simulated 12-day total precipitation at grid points containing one or more raingauge stations. The solid line indicates the perfect fit between the grid-

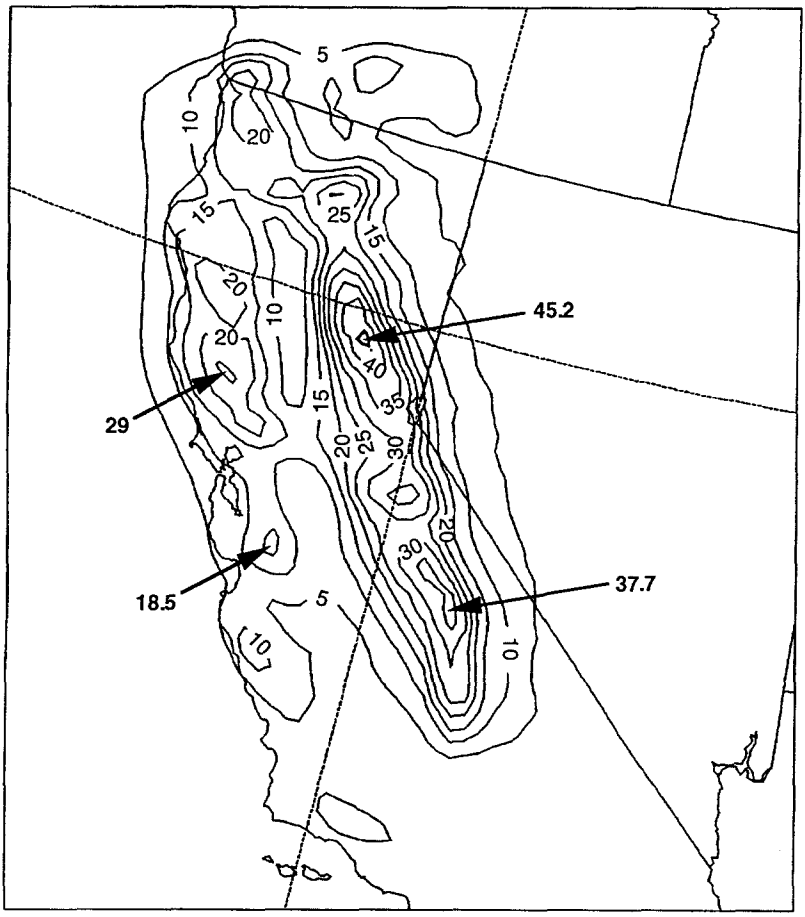

Fig. 5. The simulated 12-day total precipitation.

point and raingauge data. Factor-of-two agreements between the grid-point and raingauge data are represented by the two dashed lines. The simulated grid-point precipitation is generally in good agreement with the observed raingauge data as most of the simulated grid-point precipitation values agreed with the raingauge data within a factor of two. We obtained a correlation of 0.87 between the grid-point precipitation and raingauge data presented in Figure 6. Much of the scatter in this comparison may have been caused by comparing the area-averaged values (grid-point precipitation) and the point observations (raingauge data). Precipitation data measured by two different raingauges only a few kilometers apart from each other differed frequently by a factor of two or more. In general, the model slightly overestimated the observed precipitation over the entire range of the observed precipitation values.

To further evaluate the simulated precipitation for topographic effects, we computed the mean grid-point and raingauge precipitation within three subregions: the

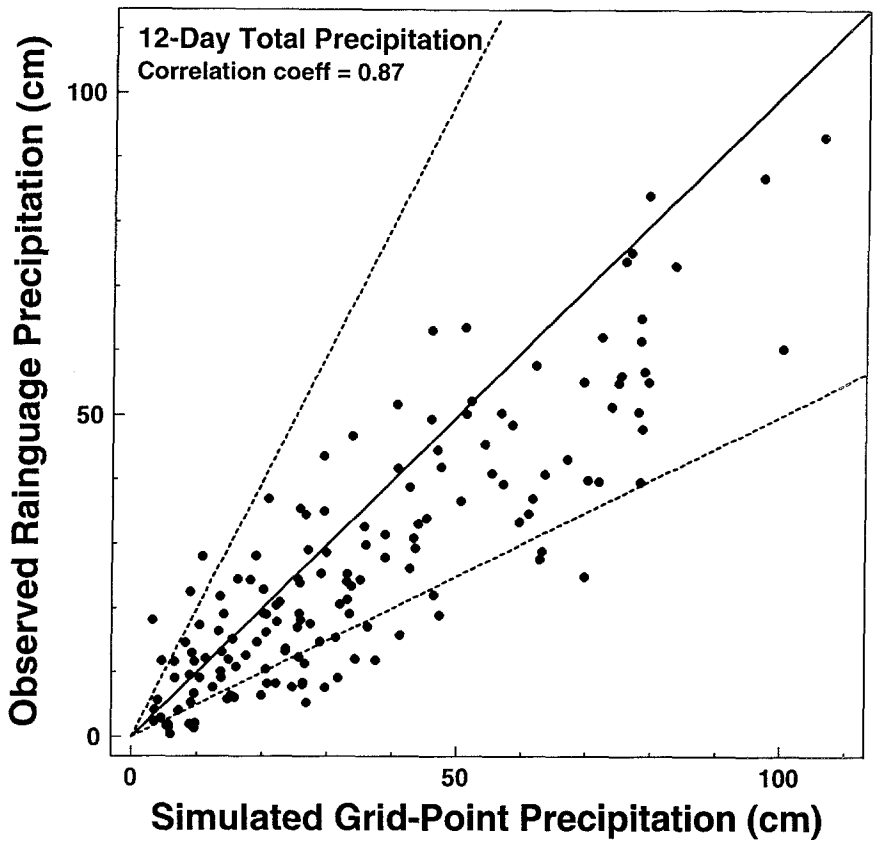

Fig. 6. A comparison of the 12-day total rain gauge and grid-point precipitation.

Coastal Range, Central Valley, and Sierra Nevada Mountains. The total precipitation within each subregion (Figure 7), both from the simulation and raingauge data, displayed the expected spatial variations associated with the regional topography. The heaviest precipitation occurred over the Sierra Nevada region and the weakest precipitation was over the Central Valley area. The simulated grid-point precipitation agreed well with the raingauge precipitation data within individual subregions with differences less than 10% of the observed values.

Major mountain ranges in California are approximately perpendicular to paths of winter storms which usually approach from the Pacific Ocean. Therefore, as shown in Figures 3 and 5, precipitation in California varies significantly in the west-east direction due to orographic lifting at upstream sides and rainshadow effects associated with descending motions at lee sides of major mountain ranges. These orographic effects on the local precipitation are well illustrated in the distributions of the total condensate which include cloud water, cloud ice, raindrops, snow, and graupel (Figure 8a), vertical velocity (Figure 8b), and precipitation (Figures 8c, d) at a x-z cross section. The location of the cross-section shown in Figure 8 is

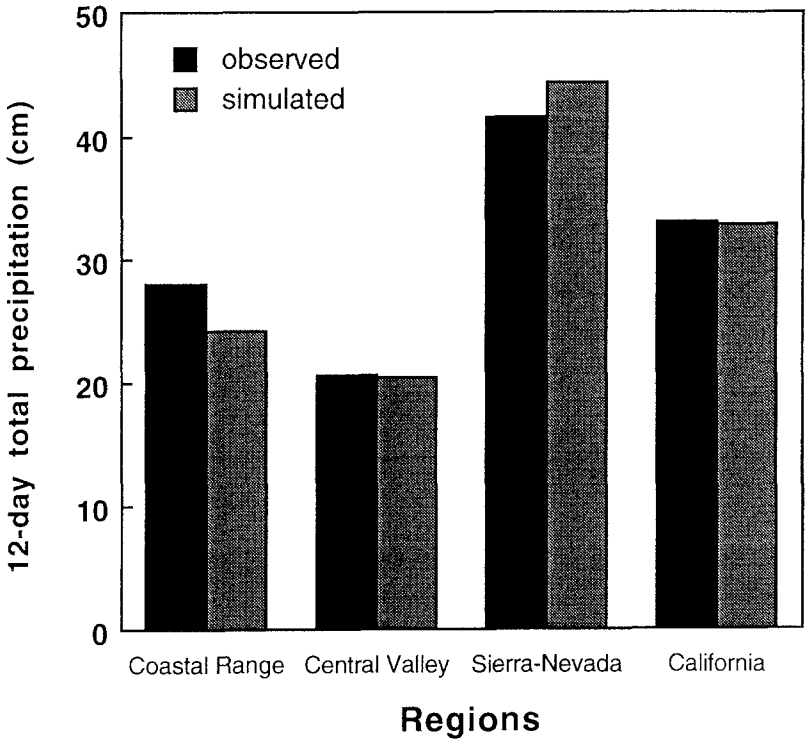

Fig. 7. The 12-day total precipitation over the Coastal Range (average of 63 grid points and 66 rain gauges), Central Valley (average of 31 grid points and 32 rain gauges), Sierra Nevada (average of 67 grid points and 67 rain gauges), and entire California (average of 161 grid points and 165 rain gauges).

indicated with a dashed line in Figure 2. Maximum concentration of condensed water, strongest updrafts, and heavy rainfall (and snowfall) appeared over the western slopes of the Coastal Range and the Sierra Nevada Mountains. Over the lee slopes of these mountain ranges, amounts of condensed water and precipitation decreased sharply in response to downdrafts (or local minima in updrafts). Figure 8c shows strong dependency of the surface rainfall (solid line) and snowfall (dashed line) distributions on topographic elevations as discussed in the following. The total precipitation that combines the rainfall and snowfall occurred near the ridge of the Sierra Nevada (Figure 8d). The role of ice-phase processes in shifting the precipitation toward the ridge line will be discussed in a future publication.

Figures 9 and 10 illustrate spatial distributions of the simulated twelve-day total rainfall and snowfall. Rainfall and snowfall distributions closely followed topographic elevations. The heaviest rainfall occurred within a narrow band along the middle of the western slope of the Sierra Nevada Mountains at approximately 1 km above sea level (Figure 9). At higher elevations, rainfall decreased rapidly and snowfall dominated rainfall. Locations of the maximum snowfall approximately

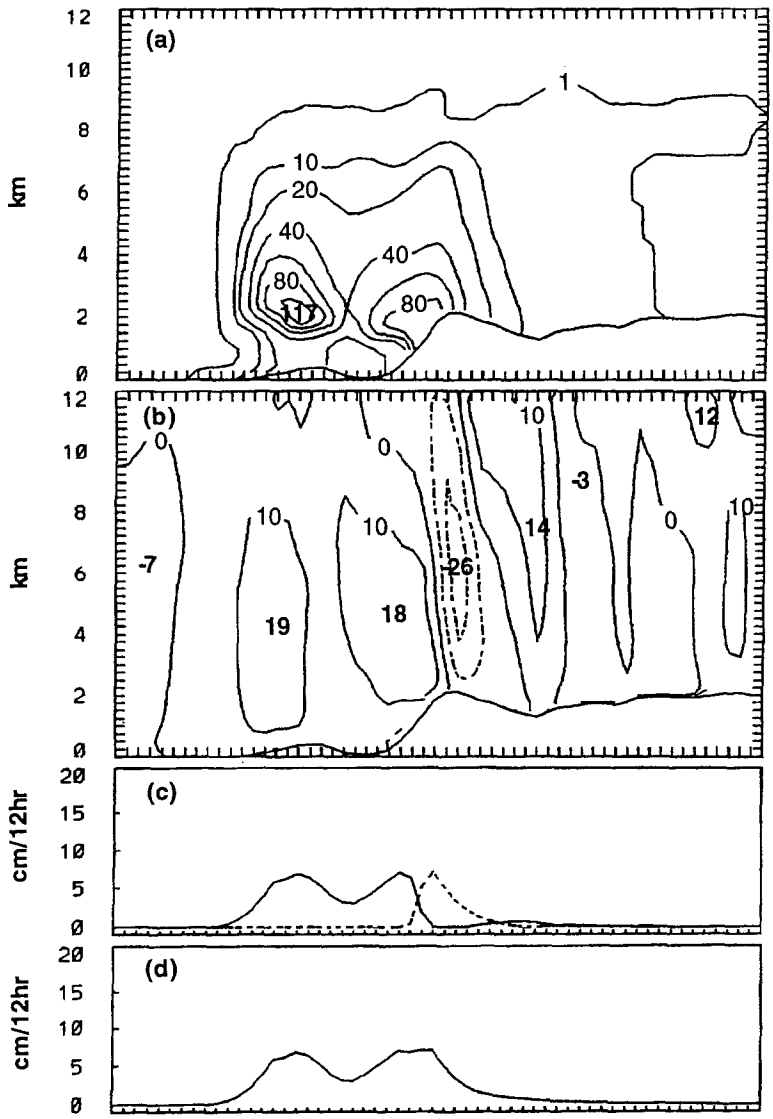

Fig. 8. Vertical cross-sections of: (a) Concentration (10^{-2} g/kg) of the total condensed water (cloud water, cloud ice, rain, snow, and graupel); and (b) vertical velocity (cm/s) at 12UTC 15 February: 12-hour (00-12UTC, 15 February) accumulated; (c) rainfall (solid line) and snowfall (dashed line); and (d) precipitation (rainfall + snowfall) along the dashed line shown in Figure 2.

coincide with the ridge line of the Sierra Nevada. The snowline, defined approximately by the 5 cm contour line in Figure 10, appeared at elevations as low as the 750 m level. At elevations above 1.8 km, snow was the dominant form of precipitation. Another rather broad band of precipitation maxima appeared along the northern and central coast of California.

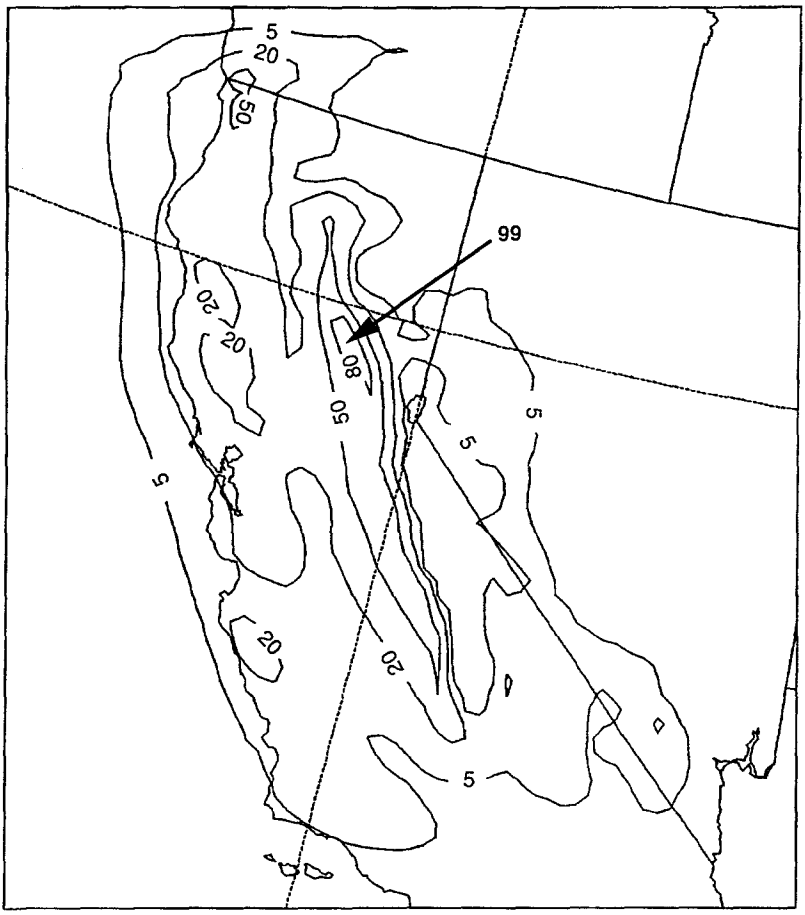

Fig. 9. The simulated 12-day total rainfall (cm).

Amounts of snow accumulated during the simulation was strongly dependent on topographic elevation since heavy snowfall and less snowmelt occurred at high elevations. As a result, significant amounts of fresh snowfall over high grounds of the Sierra Nevada Mountains were added to the existing snow accumulation (Figure 11) during the period.* Figure 12 illustrates the amount of snowmelt over the simulation period. Much of fresh snowfall over low elevations had melted at the end of the simulation period. The ratio of the snow accumulated at the end of the simulation period to the total snowfall during the twelve-day period (Figure 13) indicates a strong dependence of snowmelt on topographic elevations. Due to the decrease of the atmospheric temperature with increasing altitude, only a small portion of fresh snowfall melted at high elevations. Over the central Sierra Nevada

* Since the amount cover at the beginning of the simulation period was not known, the accumulated snow illustrated in Figure 12 represents the net increase of snow cover during the twelve-day period.

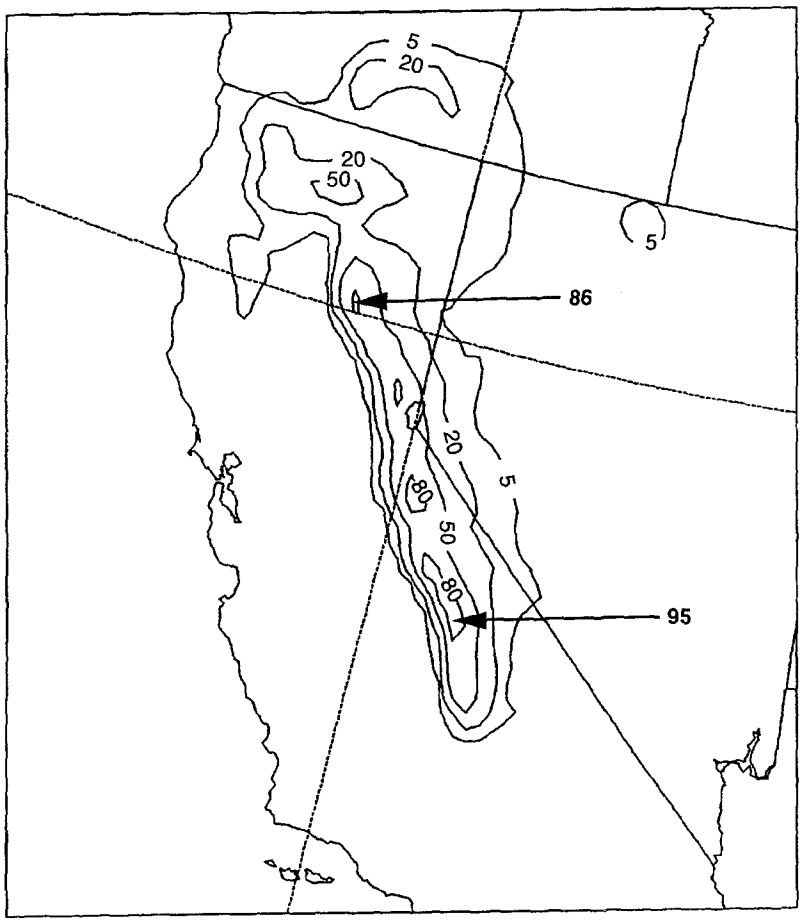

Fig. 10. The simulated 12-day total snowfall (cm of water).

at elevations higher than 1.5 km above sea level, more than 75% of the fresh snowfall during the simulation period was added to the existing snowpack.

6. Conclusion

We have presented the simulated wintertime precipitation during 11–22, February 1986 heavy precipitation in California. With the initial and time-dependent lateral boundary conditions obtained from the twice-daily NMC global analysis, the Mesoscale Atmospheric Simulation (MAS) model has successfully simulated important features of the observed precipitation such as the spatial and temporal distributions of precipitation.

The observed and simulated precipitation show two important factors that determine the precipitation in California: the large-scale water vapor budget and local

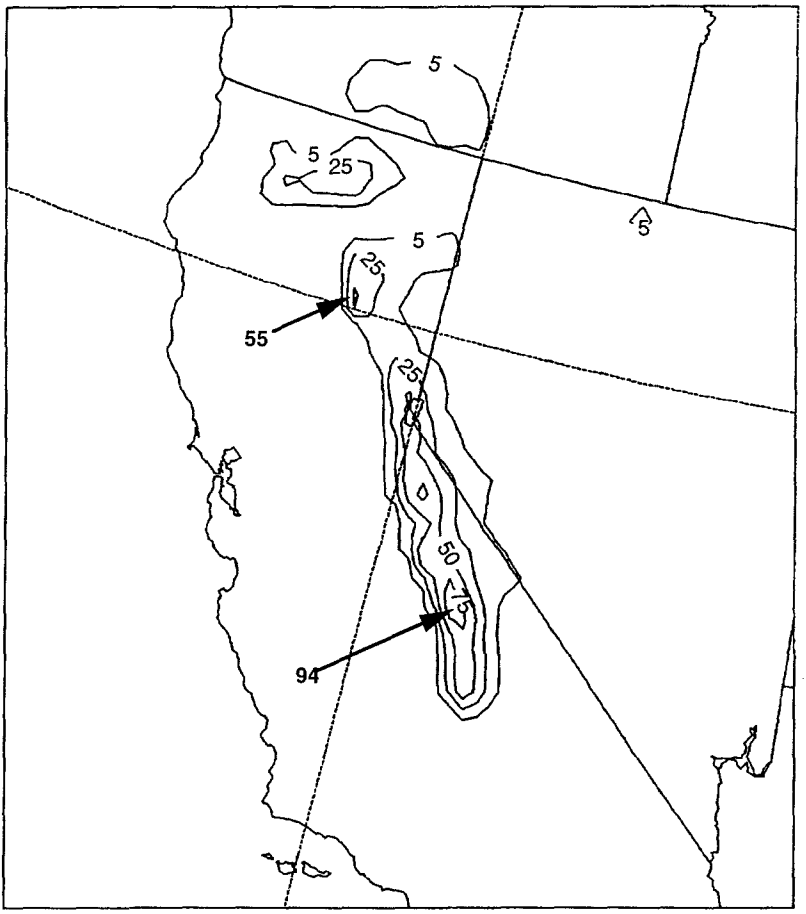

Fig. 11. The simulated 12-day total snow accumulation (cm of water).

topography. Close correlation between the temporal variations of water vapor convergence within the region derived from the NMC global analysis and the observed daily precipitation over California suggests that the NMC global analysis, that was used to drive the simulation, accurately represented the large-scale moisture budget over the model domain during the simulation period. The simulated daily precipitation is closely correlated with the observed daily precipitation and with the large scale moisture budget derived from the NMC analysis. This suggests that a Davies-type lateral boundary condition accurately represented temporal variations of the large scale flow for this simulation.

Topography appeared to be the most important local element which determines the winter precipitation and hydrology in California. The occurrence of heavy precipitation along the western slopes and ridge lines of the major mountain ranges, the Sierra Nevada and the Coastal Range, indicates that precipitation in the region is mainly caused by the orographic lifting of the oceanic inflow at the upslopes

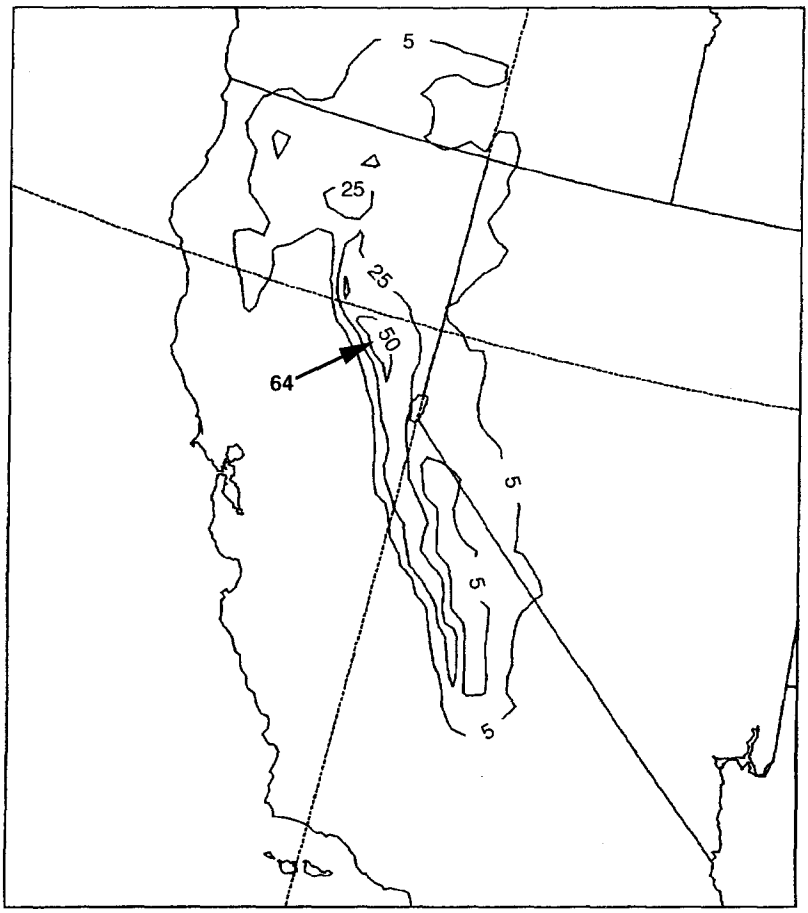

Fig. 12. The simulated snowmelt over the 12-day period (cm of water).

of major mountain ranges. Rainshadow effects caused weaker precipitation within the Central Valley area.

Another important role of topography is partitioning the total precipitation into rainfall and snowfall. The snowline during the study period appeared at elevations as low as 750 m above level and snow was the dominant form of precipitation at elevations above the 1.8 km level. Since the Sierra Nevada Mountains extend above the 3 km level, a significant portion of the total precipitation over the Sierra Nevada area was in the form of snow. In fact, the precipitation maxima along the ridge of the Sierra Nevada Mountains is due to snowfall. The simulation also suggests that over 75% of the fresh snowfall at elevations above 1.5 km level was added to the pre-existing snowpack. On the other hand, most of the fresh snowfall at lower elevations melted and did not contribute to increasing the existing snow cover.

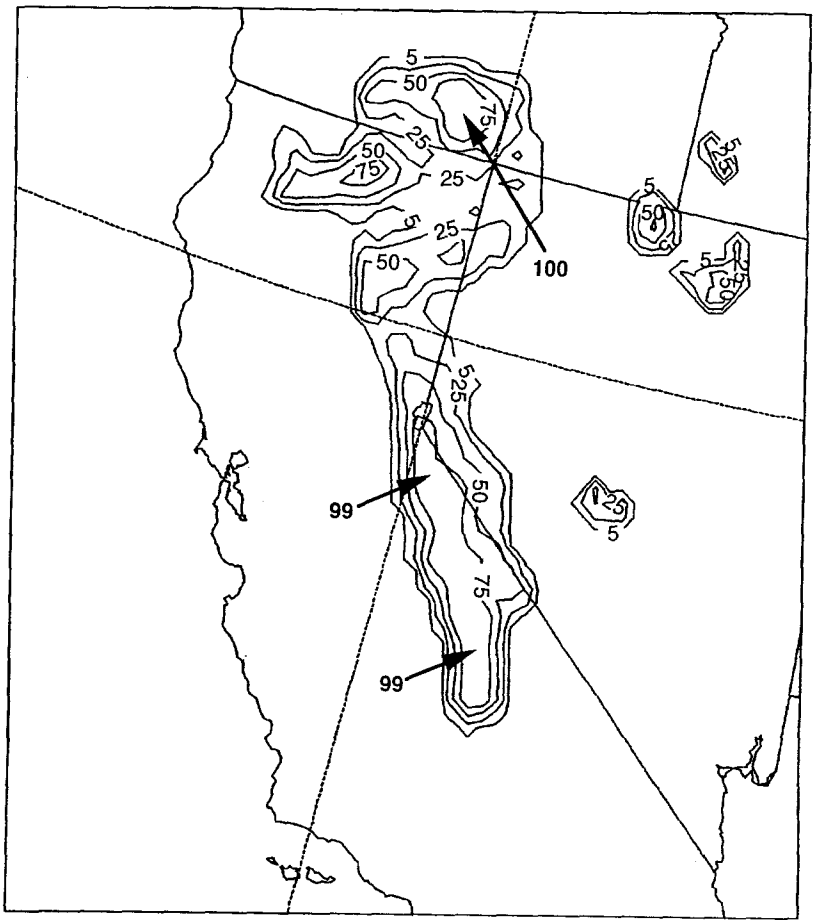

Fig. 13. The ratio (%) between the simulated 12-day total snow accumulation and the 12-day total fresh snowfall.

Acknowledgements

We thank Dr. John Roads of Scripps Institution of Oceanography for providing the raingauge data and for careful review of this manuscript. Bill Mork of California Dept. of Water Resources provided precipitation analysis map. Suggestions by Drs. Marvin Dickerson and John Leone of Lawrence Livermore National Lab. were also valuable. This work is supported by National Institute for Global Environmental Change under the grant W/GEC0017, Institutional Collaborative Research Program of Univ. of California, and Laboratory Directed Research and Development Program of Lawrence Livermore Nat. Laboratory. The National Supercomputing Center for Energy and the Environment provided computational resources to complete this work. Work performed under the auspices of the U.S. Dept. of Energy by

the Lawrence Livermore National Laboratory under contract No. W–7405–Eng–48.

References

Anthes, R. and Warner, T.: 1978, 'Development of Hydrostatic Models Suitable for Air Pollution and Other Meteorological Studies', *Mon. Wea. Rev.* **106**, 1045–1078.

Arakawa, A.: 1986, *Physically-Based Modeling and Simulation of Climate and Climate Change*, Schlesinger, M. E. (ed.), Kluwer Academic Publishers, 624 pp.

Arakawa, A. and Suarez, M.: 1983, 'Vertical Differencing of the Primitive Equations in Sigma Coordinates', *J. Atmos. Sci.* **111**, 34–45.

Chen, S.-C., Roads, J. O., Juange, H., and Kanamitsu, M.: 1994, 'California Precipitation Simulation in the Nested Spectral Model: 1993 January Event', *Proceedings for Predicting Heavy Rainfall Events in California: A Symposium to Share Weather Pattern Knowledge, 25 June 1994, Rocklin, CA.*

Cho, H.-R. and Iribarne, J.: 1987, 'The Role of Clouds and Precipitation in Long-Range Transport and Acid Rain in Canada. Phase II: Programming, Testing and Refining of Cloud Dynamics, Microphysics and Chemistry Models. Vol. 2, Appendix I: Cloud Microphysics', Report for the Canadian Electrical Assoc., Res. and Development.

Cho, H., Niewiadomski, M., and Iribarne, J.: 1989, 'A Model of the Effect of Cumulus Clouds on the Redistribution and Transformation of Pollutants', *J. Geophys. Res.* **94**, No. D10, 12895–12910.

Choularton, T. and Perry, S.: 1986, 'A Model of the Orographic Enhancement of Snowfall by the Seeder-Feeder Mechanism', *Q. J. Roy. Meteorol. Soc.* **112**, 113–129.

Cressman, G.: 1959, 'An Operational Objective Analysis System', *Mon. Wea. Rev.* **87**, 367–374.

Davies, H.: 1976, 'A Lateral Boundary Formulation for Multi-Level Prediction Models', *Q. J. Roy. Meteorol. Soc.* **102**, 404–418.

Davis, R.: 1982, *Documentation of the Solar Radiation Parameterization in the GLAS Climate Model*, NASA Tech. Memo., 83916, NASA GSFC, Greenbelt, Maryland, 57 pp.

Deardorff, J. W.: 1978, 'Efficient Prediction of Ground Surface Temperature and Moisture, with Inclusion of a Layer of Vegetation', *J. Geophys. Res.* **83**, No. C4, 1889–1903.

Department of Water Resources, California: 1988, *California High Water: 1985–1986*, Bulletin 69–86, May 1988, Department of Water Resources, State of California, 107 pp.

Dickinson, R. E., Errico, R. M., Giorgi, F., and Bates, G. T.: 1989, 'A Regional Climate Model for the Western United States', *Clim. Changes* **15**, 383–422.

Dudhia, J.: 1989, 'Numerical Study of Convection Observed During the Winter Monsoon Experiment Using a Mesoscale Two-Dimensional Model', *J. Atmos. Sci.* **46**, 3077–3107.

Ek, M. and Mahrt, L.: 1991, *OSU 1-D PBL Model User's Guide*, Dept. of Atmos. Sci., Oregon State Univ., Corvallis, Oregon, 118 pp.

Ellingson, R. G., Ellis, J., and Fels, S.: 1991, 'The Intercomparison of Radiation Codes Used in Climate Models: Long Wave Results', *J. Geophys. Res.* **96**, No. D5, 8929–8953.

Errico, R. M. and Baumhefner, D. P.: 1987, 'Predictability Experiments Using a High Resolution Limited Area Model', *Mon. Wea. Rev.* **114**, 1625–1641.

Giorgi, F.: 1990, 'Sensitivity of Wintertime Precipitation and Soil Hydrology Simulation over the Western United States to Lower Boundary Specifications', *Atmos. Ocean.* **1**, 1–23.

Giorgi, F.: 1991, 'Sensitivity of Simulated Summertime Precipitation over the Western United States to Different Physics Parameterization, *Mon. Wea. Rev.* **119**, 2870–2888.

Giorgi, F. and Bates, G. T.: 1989, 'The Climatological Skill of a Regional Model over Complex Terrain', *Mon. Wea. Rev.* **117**, 2325–2347.

Giorgi, F., Bates, G. T., and Nieman, S. J.: 1993a, 'The Multiyear Climatology of a Regional Atmospheric Model over the Western United States', *J. Clim.* **6**, 75–95.

Giorgi, F., Marinucci, M. R., and Bates, G. T.: 1993b, 'Development of a Second-Generation Regional Climate Model (RegCM2). Part II: Convective Processes and Assimilation of Lateral Boundary Conditions', *Mon. Wea. Rev.* **121**, 2814–2832.

Haltiner, G. J. and Williams, R. T.: 1980, *Numerical Prediction and Dynamic Meteorology*, John Wiley & Sons, New York, 477 pp.

Harshvardahn and Corsetti, T.: 1984, *Longwave Radiation Parameterization for the UCLA/GLAS GCM*, NASA Tech. Memo. 86072, NASA GSFC, Greenbelt, Maryland, 33 pp.

Harshvardhan, Davies, R., Randall, D. A., and Corsetti, T.: 1987, 'A Fast Radiation Parameterization for Atmospheric Circulation Models', *J. Geophys. Res.* **92**, No. D1, 1009–1016.

Hsu, Y.-J. and Arakawa, A.: 1990, 'Numerical Modeling of the Atmosphere with an Isentropic Vertical Coordinate', *Mon. Wea. Rev.* **118**, 1933–1959.

Kim, J., Ek, M., and Lee, B. L.: 1994, 'A Long-Term Simulation of Surface Fluxes and Soil Moisture', *Proceedings of the 6th Conference on Climate Variations*, 23–28 January 1994, Nashville, TN.

Kim, J. and Mahrt, L.: 1992, 'Simple Formulation of Turbulent Mixing in the Stable Free Atmosphere and Nocturnal Boundary Layer', *Tellus* **44A**, 381–394.

Krishnamurti, T., Ramanathan, Y., Pan, H.-L., Pasch, R., and Molinary, J.: 1980, 'Cumulus Parameterization and Rainfall Rates I', *Mon. Wea. Rev.* **108**, 465–472.

Kuo, H. L.: 1965, 'On Formation and Intensification of Tropical Cyclones through Latent Heat Release by Cumulus Convection', *J. Atmos. Sci.* **22**, 40–63.

Lacis, A. A. and Hansen, J. J. E.: 1974, 'A Parameterization for the Absorption of Solar Radiation in the Earth's Atmosphere', *J. Atmos. Sci.* **31**, 118–133.

Lin, Y., Farley, R., and Orville, H.: 1983, 'Bulk Parameterization of the Snow Field in a Cloud Model', *J. Clim. Appl. Met.* **22**, 1065–1092.

Louis, J. F., Tieke, M., and Gelevyn, J.: 1981, 'A Short History of the Operational PBL-Parameterization at ECMWF', *Workshop on Planetary Boundary Parameterization*, 59–79, ECMWF, 260 pp.

Mahrt, L. and Pan, H.-L., 1984, 'A Two-Layer Model of Soil Hydrology', *Bound-Layer Met.* **29**, 1–20.

Roads, J. O., Chen, S.-C., Guetter, A. K., and Georgakakos, K. P.: 1994, 'Large-Scale Aspects of the United States Hydrologic Cycle', *Bull. Amer. Met. Soc.* **75**, 1589–1610.

Roads, J. O., Maisel, N., and Alpert, J.: 1991, 'Further Evaluation of the National Meteorological Center's Medium Range Forecast Model Precipitation Forecasts', *Weather Forecast.* **6**, 483–497.

Starr, D. and Cox, S.: 1985, 'Cirrus Clouds. Part I: A Cirrus Cloud Model', *J. Atmos. Sci.* **42**, 2663–2681.

Stephens, G.: 1978, 'Radiation Profiles in Extended Water Clouds. II: Parameterization Schemes', *J. Atmos. Sci.* **35**, 2123–2132.

Takacs, L. L.: 1985, 'A Two-Step Scheme for the Advection Equation with Minimized Dissipation and Dispersion Errors', *Mon. Wea. Rev.* **113**, 1050–1065.

Wallace, J., Tibaldi, S., and Simmons, A.: 1983, 'Reduction of Systematic Forecast Errors in the ECMWF Model through the Introduction of an Envelope Orography', *Q. J. Roy. Meteorol. Soc.* **109**, 683–717.

Zhang, D.-L. and Fritsch, J. M.: 1988, 'A Numerical Investigation of a Convectively Generated, Inertially Stable, Extratropical Warm-Core Mesovortex over Land. Part I: Structure and Evolution', *Mon. Wea. Rev.* **116**, 2660–2687.

Zhang, D.-L. and Gao, K.: 1989, 'Numerical Simulation of an Intense Squall Line During 10–11 June 1985 Pre-Storm. Part II: Rear Inflow, Pressure Perturbations and Stratiform Precipitation', *Mon. Wea. Rev.* **117**, 2067–2094.

Zhang, D.-L., Gao, K., and Parson, D.: 1989, 'Numerical Simulation of an Intense Squall Line During 10–11 June 1985 Pre-Storm. Part I: Model Verification', *Mon. Wea. Rev.* **117**, 960–994.

Zhang, D.-L., Hsie, E.-Y., and Moncrieff, M.: 1988, 'A Comparison of Explicit and Implicit Predictions of Convective and Stratiform Precipitating Weather Systems with a Meso-β-Scale Numerical Model', *Q. J. Roy. Meteorol. Soc.* **114**, 31–60.

Zobler, L.: 1986, *A World Soil File for Global Climate Modelling*, NASA Tech. Memo. 87802.

(Received 11 January, 1995; in revised form 30 May, 1995)